METRICA
METRology Institutional CAtalog

ISTITUTO NAZIONALE DI RICERCA METROLOGICA
Repository Istituzionale

Direct calibration of a true-rms ac voltmeter against a He-free pulsed Josephson standard

Original
Direct calibration of a true-rms ac voltmeter against a He-free pulsed Josephson standard / Kubiczek, Krzysztof; Durandetto, Paolo; Capra, Pier Paolo; Francese, Claudio; Lanzillotti, Marco; Roncaglione, Luca; Kampik, Marian; Sosso, Andrea. - In: MEASUREMENT. - ISSN 0263-2241. - 236:(2024). [10.1016/j.measurement.2024.114981]

Availability:
This version is available at: 11696/81139 since: 2024-06-11T08:16:09Z

Publisher:
Elsevier

Published
DOI:10.1016/j.measurement.2024.114981

Terms of use:

This article is made available under terms and conditions as specified in the corresponding bibliographic description in the repository

Publisher copyright

(Article begins on next page)

30 June 2024

Measurement 236 (2024) 114981

Contents lists available at ScienceDirect

Measurement

journal homepage: www.elsevier.com/locate/measurement

Direct calibration of a true-rms ac voltmeter against a He-free pulsed Josephson standard

Krzysztof Kubiczek [a,*], Paolo Durandetto [b], Pier Paolo Capra [b], Claudio Francese [b], Marco Lanzillotti [b], Luca Roncaglione [b], Marian Kampik [a], Andrea Sosso [b]

[a] Department of Measurement Science, Electronics and Control, Faculty of Electrical Engineering, Silesian University of Technology, Akademicka 2A, Gliwice, 44100, Poland

[b] INRiM - Istituto Nazionale di Ricerca Metrologica, strada delle Cacce 91, Turin, 10135, Italy

ARTICLE INFO

Keywords:
Josephson arbitrary waveform standard
Thermal voltage converter
True-rms voltage calibration
Quantum metrology

ABSTRACT

Starting from 2019 a new central role is played by quantum standards, owing to the redefined SI, where electrical units are directly linked to the fundamental constants *e* (elementary charge) and *h* (Planck constant). Thus, metrologists are nowadays trying to extend the astonishing accuracy attainable in dc measurements to ac and beyond, moving towards calibrations aiming quantum ac voltage generation. Programmable Josephson Voltage Standards are nowadays capable of fulfilling primary metrology requirements only for stepwise-approximated voltage signals up to few hundreds Hz. Pulsed Josephson standards are instead capable of generating arbitrary waveforms at higher frequencies, so are generally called Josephson Arbitrary Waveform Standards (JAWS). Despite of the lower attainable voltage, JAWS are very promising and are the subject of intense research activity. In particular, the capability of generating high spectral purity signals allows high accuracy measurements especially at the low voltage levels (<100 mV rms), which are challenging to be performed by the traditional ac-dc transfer difference using thermal converters. We report in the following about our setup for quantum-based calibrations of a true-rms ac voltmeter with low uncertainty, first results obtained and unsolved issues.

1. Introduction

The impressive improvement in accuracy of dc voltage calibrations attained with Josephson junction arrays is one of the most relevant success of quantum voltage metrology [1]. Dc Josephson Voltage Standards (JVSs) are capable of generating stable voltages exceeding 10 V with uncertainties below 1 nV/V [2]. Unfortunately, the generation of ac voltages of similar accuracy is difficult because the output voltage cannot change unless at relatively low rate. Instead, the current–voltage (IV) relationship [3] in Programmable Josephson Voltage Standards (PJVSs) makes it possible to suitably control the quantum voltage by setting the junction bias current. PJVS array are realized with thousands Josephson junctions, connected in series and distributed among suitably-weighted segments. This configuration enables the total voltage across the entire array to be programmed through the current-controlled activation/deactivation of each segment. Among the different technologies proposed for PJVS, we mention the SNS junctions developed in cooperation between NIST and PTB [4,5], with respectively Nb and Nb_xSi_{1-x} as superconducting (S) and normal (N) elements, and the SNIS junctions, developed by INRiM and PTB [6], with respectively Nb, Al and AlO_x as superconducting (S), normal (N) and insulating (I) elements. The latter proved to be particularly interesting for operation with He-free systems [7].

The main limitation of PJVS lies in the time taken for the output voltage switching: during these transients, the array voltage is not quantum-defined, thereby restricting PJVS arrays to meet the requirements of primary metrology uncertainties only for signals up to a few kHz. In spite of this, PJVS have been shown capable of calibrating precision ac voltage sources using selective differential sampling techniques [8–11], achieving considerably lower uncertainties compared to thermal voltage converters (TVCs), down to one part in 10^8 at 1 V and 250 Hz [12]. Frequency extension of PJVS calibrations up to 100 kHz is also under investigation by means of differential sub-sampling [13,14].

To further get rid of PJVS limitations, arrays operating with an (ideally) square wave, pulsed microwave bias were developed. Indeed, the use short pulses rather than a continuous sinusoidal wave allows to suitably modulate the signal frequency over a wide range of frequencies [15,16]. Fundamental accuracy follows then from the control of each flux quantum, occurring when every single pulse goes through a

* Corresponding author.
E-mail address: krzysztof.kubiczek@polsl.pl (K. Kubiczek).

https://doi.org/10.1016/j.measurement.2024.114981
Received 16 February 2024; Received in revised form 16 April 2024; Accepted 21 May 2024
Available online 28 May 2024
0263-2241/© 2024 The Author(s). Published by Elsevier Ltd. This is an open access article under the CC BY-NC license (http://creativecommons.org/licenses/by-nc/4.0/).

junction: the output voltage of the array is then exactly calculable in terms of fundamental constants, since the number of the quanta per unit time, i.e. the pulse repetition rate, is accurately known. Exploiting the $\Sigma\Delta$ technique developed for semiconductor electronics [17], pulsed arrays are capable of synthesizing quantum-accurate arbitrary waveforms, earning them the title of Josephson Arbitrary Waveform Synthesizers (JAWS). Among these, high-purity and precisely calculable voltage sine waves are utilized for high-accuracy ac calibrations of both voltage sources and voltage meters. This is further explored in the following section, introducing the main topic covered in this work: the calibration of a widely used metrology-grade true-rms ac voltmeter with a cryocooled JAWS system.

2. JAWS for ac voltage calibrations

The ability of JAWS to synthesize pure signals across a broad frequency spectrum enables straightforward ac voltage calibrations with ultimate accuracy, ensured by the quantum nature of JAWS voltages. In general, the JAWS instantaneous voltage $V_J(t)$ is given by:

$$V_J(t) = \Phi_0 \, N \, n \, f_{rep}(t) \tag{1}$$

where $\Phi_0 = h/2e \simeq 2.07 \cdot 10^{-15}$ Wb is the magnetic flux quantum, N is the number of junctions in the array and n is the number of flux quanta transferred per pulse (typically $n = \pm 1$). With N being fixed, the voltage only depends on the pulse repetition frequency $f_{rep}(t)$ and on the pulse polarity, driving each junction to transfer either a positive ($n = 1$) or a negative ($n = -1$) quantum flux. Quantum-accurate arbitrary waveforms can then be synthesized by modulating the pulse density by means of $\Sigma\Delta$ algorithms, thus producing a 1/0/−1 bitstream that digitally encodes the desired signal and that is loaded on the circulating memory of a ternary PPG.

Quantum-traceable sine waves of high purity are currently considered to estimate the ac-dc transfer difference of TVCs with unparalleled accuracy for primary ac voltage metrology [18]. At present, TVCs are the most-accurate instruments in ac voltage measurements: they operate by comparing the electrical power from ac and dc voltages and determining the rms value from the heating effect of both. However, due to thermoelectric and electromagnetic effects, TVCs are affected by a residual difference of its response to ac and dc inputs, that depends on both applied voltage and frequency. The determination of this ac-dc transfer difference, expressed as the fractional difference between the ac and the dc voltages that produces the same electromotive force at the TVC output, is the main objective of the metrological characterization of each ac-dc standard [19,20].

In measurements with JAWS, owing to the direct connection to TVC, the low input impedance of TVCs is an issue for the limited current compliance of JAWS standards, so we considered a commercial ac voltage measurement standard with buffered input, whose loading effect is negligible at frequencies below 10 kHz.

In the following we report about the evaluation of the transfer difference of a Fluke 5790A[1] true-rms wideband ac voltmeter based on the thermal voltage converter (similar to that used in the Fluke 792A ac/dc transfer standard) using our cryocooled JAWS system. The latter was carefully characterized and electrically-driven towards the generation of the quantum-referenced ac voltage sine waves to be applied at the input of the device under test (DUT).

Fluke 5790A can operate in two distinct modes: (i) the "transfer mode", where it works as the Fluke 792A, thus requiring an external dc reference; (ii) the "measurement mode", which instead uses the precision internal source as dc reference. In the second, the procedure of the ac/dc switching is performed automatically by the instrument. In this article, this measurement mode was selected to calibrate the instrument.

3. Calibration setup

The calibration setup is depicted in Fig. 1. It is realized around a "flexible" cryogen-free refrigeration system [21], suited to operate both programmable and pulsed standards. It is based on a two-stage pulse-tube cryocooler[2] with 1 W cooling power at 4 K and minimum temperature below 3 K (without thermal loads). The second stage is fitted with an additional oxygen-free high thermal conductivity (OFHC) copper disk (the coldplate, henceforth) to increase the useful cold surface of the bare cold head. A low-thermal resistance cryopackage, similar to that presented in [22], hosts the JAWS chip and is tightly screwed onto the coldplate. The JAWS sample consists of two arrays, with 5000 SNS junctions each (a single array is depicted in Fig. 1), manufactured by PTB with Nb_xSi_{1-x} as N material [23] and both thickness and Nb/Si relative content (x) trimmed to achieve characteristic frequencies around 10 GHz–15 GHz at 4.2 K. At this temperature, the critical current is equal to about 5 mA, while the normal resistance of the array is about 20 Ω i.e. 4 mΩ per junction. Junctions are arranged in double stacks and each array is embedded into the center line of a 50 Ω coplanar waveguide (CPW), terminated with a matched resistor. A Rogers 3006 PCB allows the interconnections with the JAWS chip via aluminum bonding wires and with the broadband coaxial cable through an SMA launcher [24]. Two cryogenic sensors and a commercial controller[3] are used to monitor the temperature of coldplate and of the cryopackage. Additionally, the actual chip temperature can be monitored and controlled as well by using the second Josephson array as temperature sensor, exploiting the method presented in [25].

The high frequency pulsed signal is generated by a PPG Anritsu MU183020A module, installed on a MP1800A mainframe. The PPG is equipped with four channels, each providing two-level Non-Return-to-Zero (NRZ) pulsed patterns up to 28 Gbit s^{-1}. The required Return-to-Zero (RZ) patterns are then obtained by purposely inserting a '0' digit, thus reducing the maximum pulse repetition frequency to 14 GHz. With a binary pattern, corresponding to logical '0' and '1', JAWS standards can only synthesize unipolar waveforms. Two independent PPG channels are then combined with a 6 dB power splitter to obtain the three-state logical outputs ('−1', '0', '1') required to synthesize bipolar waveforms [26].

The combined pulsed stream from the two channels is then transmitted to the JAWS array through a low-thermal conductivity and 30 GHz bandwidth coaxial cable, with center and outer conductor made of silver-plated beryllium copper and beryllium-copper, respectively. To further reduce the thermal load to the 4 K stage, the coaxial cable is thermally-anchored to the 40 K heat exchanger of the cryocooler through a copper link.

As shown in Fig. 1, an in/out dc-block is inserted between the coaxial cable and the JAWS circuit, making the latter electrically decoupled from the PPG and preventing the appearance common-mode voltages across the CPW termination resistor. The filtered low-frequency portion of the pulsed signal, crucial for the proper functioning of the junctions as a pulse quantizer, is then fed back to the array as a compensation current through the low-frequency bias lines, provided by an Arbitrary Waveform Generator (AWG),[4] thereby implementing the well-known "ac-coupling technique" [27]. A microwave synthesizer[5] provides the 14 GHz timebase required by the PPG as well as the 10 MHz synchronization signal to the AWG. The quantum voltage across the JAWS array is transferred to the room temperature environment through a 60 cm long twisted pair (TP) cable and an SMA vacuum-tight feedthrough installed onto an electrically insulated flange of the cryocooler vacuum chamber. In order to reduce common-mode

[1] Brand names are used for identification purposes, such use implies neither endorsement by INRiM nor assurance that the equipment is the best available in the market.

[2] Cryomech PT-410.

[3] Lake Shore 350.

[4] Agilent 33220A.

[5] DS Instruments SG30000PRO.

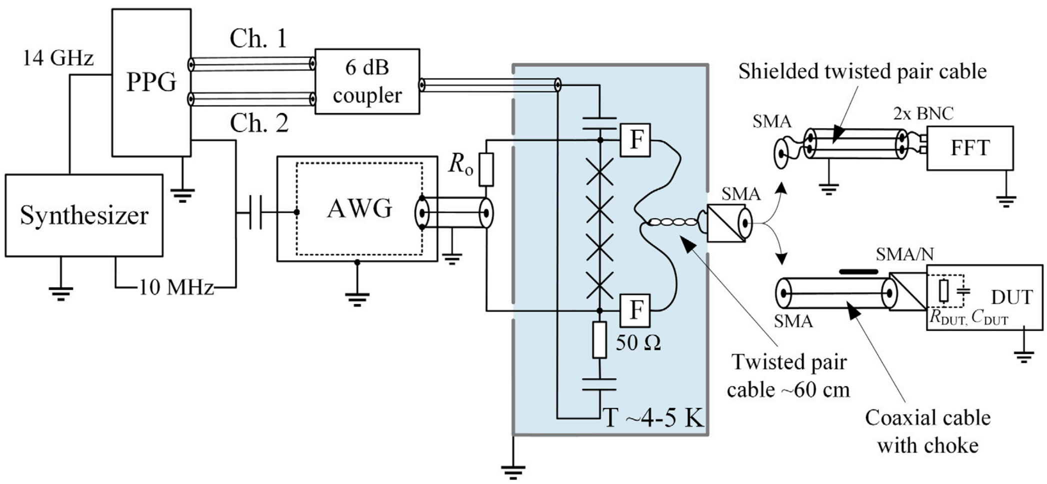

Fig. 1. Schematic representation of JAWS setup. Channel 1 and Channel 2 of the PPG respectively provide positive and negative pulses, which are then combined with the 6 dB coupler and finally transmitted to the JAWS standard in the cryogenic environment. Parallel input resistance and capacitance of the DUT are indicated as R_{DUT} and C_{DUT} and equal to 10 MΩ and 100 pF, respectively.

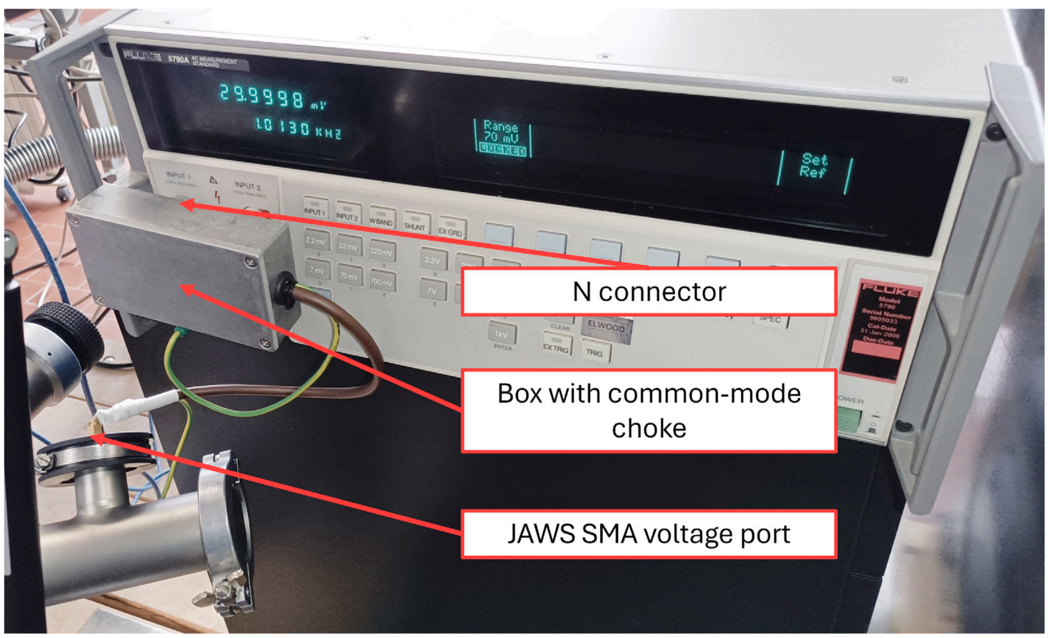

Fig. 2. Picture showing the connection between the JAWS SMA port on the cryocooler vacuum chamber and the N-input of the DUT through a common-mode choke.

noise at the DUT input, a common-mode choke has been realized by winding the coaxial cable delivering the JAWS voltage signal a few times around toroidal core and placed between the output of the vacuum-tight cryostat feedthrough and the DUT input (Fig. 2).

The AWG and an additional output resistor ($R_{\mathrm{o}} \sim 500\,\Omega$) provide a programmed current waveform with variable frequency, phase shift and amplitude up to about 20 mA. The AWG is connected to the 10 MHz reference signal from the synthesizer by a BNC-dc block (inner/outer), as a way of decoupling common grounding from the bias current [28]. A 24-bit digitizer[6] is employed as an FFT analyzer to check spectral purity and quantum-locking ranges (QLRs) [29] of the synthesized sine waves. The latter are essential to guarantee the effective quantum-traceability of the synthesized voltage waveforms

All devices in the measurement system are powered from the mains through an insulation transformer with a single grounding point. The FFT spectrum analyzer was connected to cryocooler JAWS voltage port using a shielded twisted pair cable, with its outer shielding connected to the common grounding point.

4. JAWS preliminary setting

This section outlines the experimental procedures we conducted to establish optimal environmental and bias conditions to operate our JAWS array towards the synthesis of spectrally-pure ac voltage signals. We began by observing dc quantum voltage steps at fixed pulse repetition frequencies, to determine a suitable working temperature to fully exploit the available pulse amplitude (Section 4.1). Subsequently, we studied the JAWS array response under a $\Sigma\Delta$-modulated pulsed stream, to initially setting amplitude and relative phase of the compensation current signal. (Section 4.2). Fine adjustment of bias parameters and verification of corresponding QLRs are subsequently performed through spectral analysis, as detailed in the next section (Section 5).

[6] Zurich Instruments MFLI 6236, MF-DIG Digitizer Opt.

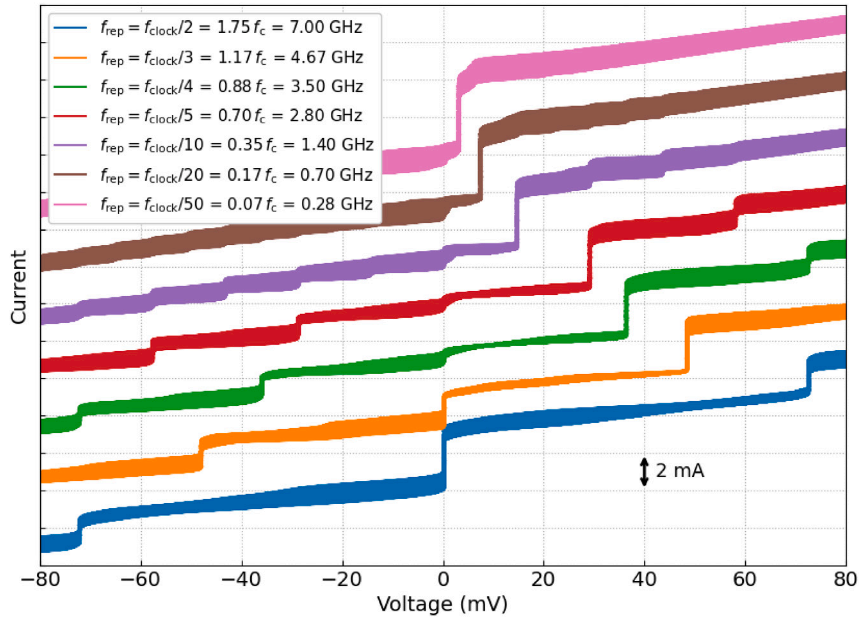

Fig. 3. IV characteristics of the JAWS array at 5.2 K under pulse streams at different repetition frequencies, ranging from $f_{\text{clock}}/2$ to $f_{\text{clock}}/50$, with $f_{\text{clock}} = 14$ GHz. Thicker traces are due to the cryocooler temperature fluctuations. Curves are vertically-shifted for clarity.

4.1. JAWS under single frequency pulsed streams

Preliminary operations with the cryocooled JAWS consist in the identification of the best operating point, i.e. optimal temperature, junctions critical current, pulse frequency and power. Owing to the several parameters under control (temperature, pulse frequency and amplitude), finding the optimal combination is nontrivial. First, properly setting the array temperature is fundamental, being junctions electrical parameters strictly dependent on temperature, especially as regards the critical current (I_c), which generally shows a steep rise with decreasing temperatures. As a consequence, the temperature setpoint also influences the junctions quantum-locking behavior under microwave irradiation. It is known indeed from [16] that QLRs of pulse-driven Josephson junctions are enhanced for high-amplitude current pulses (about $3\,I_c$) and for f_{rep} lower than the characteristic frequency $f_c = K_J \cdot I_c \cdot R_n$, with K_J and R_n the Josephson constant and the junctions normal resistance, respectively.

Due to limitations in the peak-to-peak pulse amplitude from each PPG channel (3.5 V at most) and attenuation through a 6 dB coupler, cables, and connectors, the available pulsed power is inadequate to operate the array at liquid helium temperature, where $I_c \simeq 5$ mA. Yet, the driving power scales with I_c and, consequently, the temperature of the JAWS array must be set above 4.2 K, resulting in a lower critical current to accommodate our pulse power capabilities.

We find the optimal operating temperature for pulse operation of our system by observing the current–voltage (IV) characteristics of the JAWS array under pulse streams of fixed amplitude (3 V) and different repetition frequencies f_{rep}, given by $f_{\text{rep}} = f_{\text{clock}}/N$ ($f_{\text{clock}} = 14$ GHz in this case) and N an integer number (Fig. 3). In this test, the PPG only generates positive unipolar pulses (Channel 2 is disabled), which then undergo high-pass filtering by the dc-block. Consequently, the pulse stream reaching the array is bipolar but asymmetrical, leading to the asymmetric IV plots depicted in the figure.

Positive first-order quantum voltage steps, from 0.7 mA to 2 mA in width, have been obtained at 5.2 K, despite the effect of the cryocooler temperature fluctuations [30] causes a 40% reduction (about 0.5 mA) of the useful quantum step width. Indeed, the employed temperature controller is not capable of suppressing thermal oscillations, which are too fast (a few Hz) for the feedback bandwidth. To address this issue, passive damping techniques [31] can be exploited to mitigate the reduction in quantum step width, though not yet implemented in the current setup.

At this temperature, $I_c \simeq 2.4$ mA and $f_c \simeq 4$ GHz. In accordance with [16], first step current amplitudes close to I_c, as well as nearly absent zero steps, are observed for $f_{\text{rep}} < 0.9\,f_c$. On the other hand, first quantum steps decrease to about 0.7 mA at $f_{\text{rep}} = 7$ GHz ($1.75\,f_c$), accompanied by the rise of zero-order steps. The latter represents the highest acceptable quantum voltage level (approximately 70 mV) that can be synthesized with our JAWS array under these experimental conditions. Enhancing the output voltage capability would be most straightforwardly achieved by employing a JAWS array with a greater number of junctions [32]. Another potential option involves operating the array at a lower temperature (resulting in a higher f_c), though this would require more demanding power requirements, that our PPG system cannot satisfy at present.

4.2. JAWS under $\Sigma\Delta$-modulated pulse streams and compensation current

The analysis presented in Section 4.1 is valuable for optimizing junction response to simple pulsed signals, aiming to maximize both quantum voltage and step current-width. The next step is to confirm suitable junction behavior in the case of a $\Sigma\Delta$-modulated pulse stream encoding the sine wave to be synthesized.

The IV characteristic takes the complex form illustrated in Fig. 4, where flat regions can only be observed corresponding to the peak voltages of the encoded waveform (approximately ±42.4 mV for a 30 mV-rms sine wave). The regions of the bias current where flat spots occur (around 2 mA in magnitude) then provide an estimate of the peaks of the compensation current signal to be reinjected into the array.

To achieve synchronous compensation, the slow triangular sweep current from the AWG is thus replaced by a sinusoidal one synchronized with the pulse stream, matching the desired output waveform's frequency and with current peak values lying within the flat spot regions in Fig. 4. The IV curve then transforms into a Lissajous-like figure similar to those illustrated in Fig. 5: when $\theta = 90°$, compensation current and pulse streams are entirely out of phase, resulting in a non-elliptical Lissajous figure. As θ decreases to 10°, the figure takes on an elliptical form, indicating that the JAWS voltage closely resembles the intended sine wave, and thereby serving as a preliminary check for QLR. By adjusting the phase to achieve a linear dependence (red

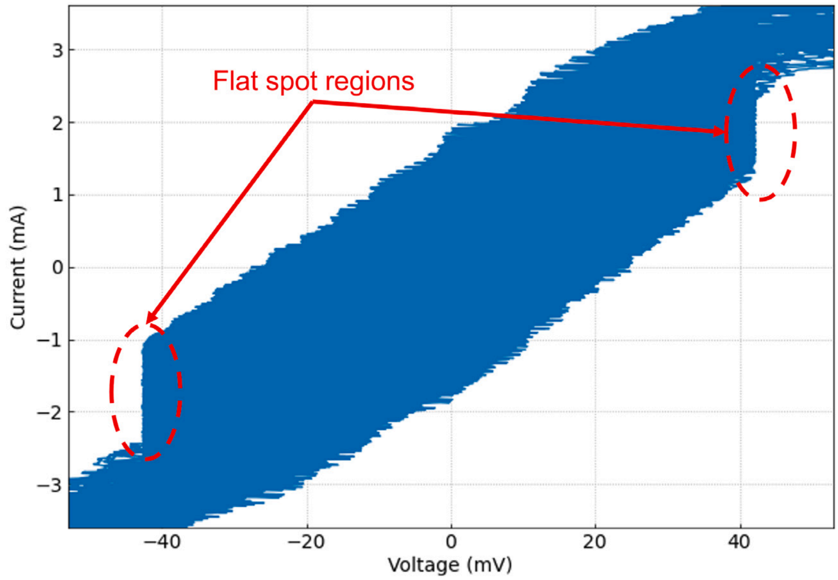

Fig. 4. IV characteristics of the JAWS array at 5.2 K under ac-coupled bipolar pulse train encoding a 1 kHz sine wave with rms voltage of 30 mV. Dashed-circles indicate the flat spots region where compensation current peaks are located, i.e. around 2 mA in magnitude.

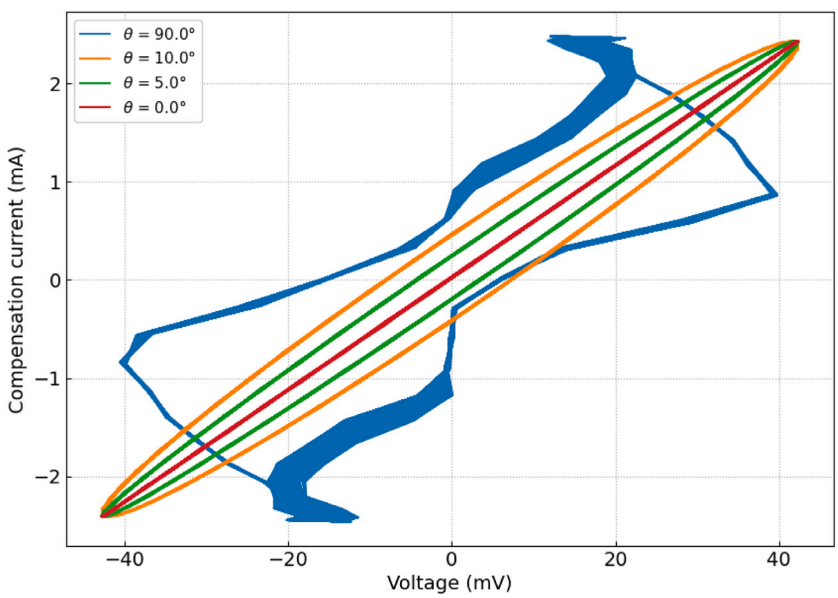

Fig. 5. Lissajous-like figures obtained by plotting compensation current vs JAWS output voltage at different relative phase values. JAWS array is radiated by a bipolar pulse train encoding a 1 kHz sine wave with rms voltage of 30 mV and current-driven by a synchronized 1 kHz sinusoidal compensation signal around 2 mA peak and relative phase θ with respect to the pulse stream.

curve), i.e., setting $\theta = 0°$, the phase is expected to be aligned closed to the center of the corresponding QLR.

It should be emphasized that, while none of the described methods serves as a comprehensive verification of QLRs, they are nevertheless useful for the initial guessing of the bias parameters. As discussed in the following section, final adjustments and QLR checks are carried out through the spectral analysis of the synthesized sine waves.

5. Results

5.1. Spectral analysis of JAWS quantum sine waves

After following the steps detailed in Section 4, we subject the JAWS voltage sine waves to spectral analysis to evaluate their spectral purity and fine-tune bias parameters. The Fast Fourier Transform (FFT) of several sine waves is depicted in Fig. 6. Higher harmonics are suppressed by at least 105 dB with respect to the fundamental tone. The noise floor above the fundamental frequency is below the level −130 dBV for the synthesized voltages with the 24-bit digitizer range set at 300 mV. As it was reported in the literature [26,33], some harmonics may appear due to nonlinearities of the sampler. We clearly observed such effect from the rise of harmonics when the operating range of the sampler was reduced for maximum amplification. The extra peaks generated by the electronics are easily noticeable in the blue line trace of Fig. 7 by comparison with the spectrum obtained with the spectrum analyzer set at higher input voltage range. Even though noise floor due to sampler is reduced by lowering range, the spurious-free-dynamic-range (SFDR) [34] is worse, so we generally avoided this condition during QLR verification measurements.

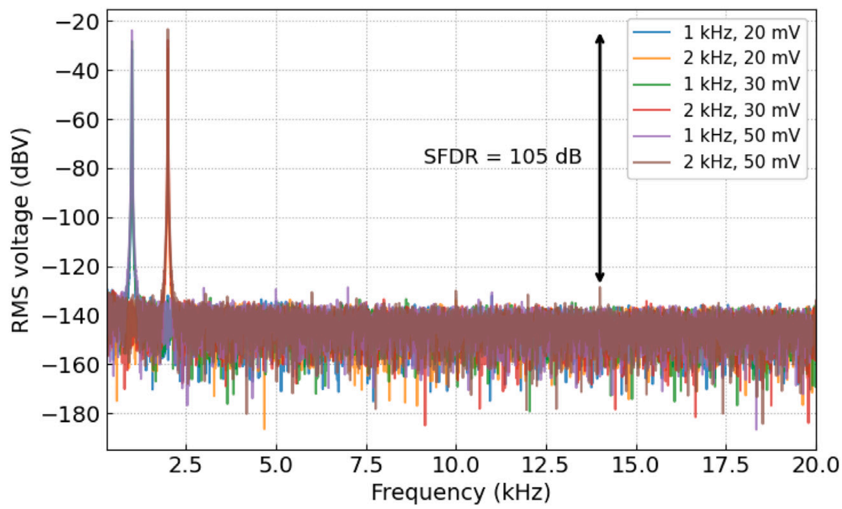

Fig. 6. Frequency spectra of quantum-based sine waves synthesized with the JAWS array at 5.2 K. The input range of the FFT analyzer was set to 300 mV. Harmonics are suppressed by at least 105 dB with respect to the fundamental tone.

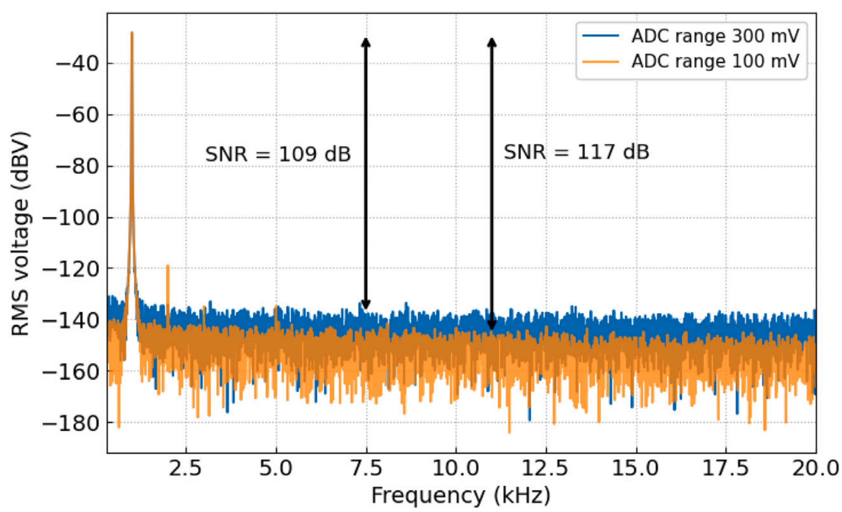

Fig. 7. Frequency spectra of a 1 kHz sine wave at 30 mV acquired at two different input ranges of the FFT analyzer.

5.2. QLR verification of JAWS sine waves

QLRs have been verified through the measurement of the total harmonic distortion (THD) of the synthesized sine waves under the variation of each of the bias parameters (amplitude of positive and negative pulses, compensation current amplitude, offset, and phase). QLRs of a 30 mV-rms sine wave at 1 kHz are illustrated in Fig. 8: red dots represent parameter values within the QLR, where THD is both minimized and quantized. The significant scattering of data points outside the QLRs (blue dots) is attributed to cryocooler oscillations, thereby verifying THD invariance under temperature variations within the QLRs. QLRs width at different JAWS voltages and frequencies is illustrated in Fig. 9.

Widest QLRs are typically measured at 300 Hz for all of the generated voltages. QLRs of positive and negative pulse amplitudes do not show any significant dependency on the frequency change (except 300 Hz while they are the widest). Their values vary between about 0.18 V (channel 1 at 20 mV rms) to about 0.6 V (channel 2 at 30 mV rms). The correlation between compensation current amplitude and the subsequent QLR offset in relation to voltage level is not readily apparent. The exception to this irregularity is 50 mV rms, for which the QLR is the narrowest for both the bias amplitude and offset.

Similarly, QLRs for the phase are related to both voltage and frequency of the synthesized waveform.

They are almost linearly dependent on the synthesized voltage, whereas they decrease from about 55° at 1000 Hz and 10 mV to below 8° for 2000 Hz and 50 mV. As reported in [35], this phenomenon is caused by the self-inductance of the JAWS array: the ac bias current generates an inductive voltage drop dependent on frequency, in quadrature with the JAWS voltage, thus reducing the phase shift margin. Such effect can also explain the voltage dependence of QLRs for compensation current amplitude and offset. Similar to the increase in frequency, increasing compensation current amplitude also leads to an enlargement of the voltage generated across the inductance of the JAWS array, thereby reducing QLRs. Further investigation is needed to understand the effect of on-chip inductance on the output voltage.

5.3. True-rms voltmeter calibration

The Fluke 5790 true-rms voltmeter has been calibrated with the cryocooled JAWS system for rms voltages from 10 mV to 50 mV and frequencies ranging from 300 Hz to 2 kHz. Calibration results are displayed in Fig. 10

Each calibration point is derived from 30 measurements taken within approximately one minute. It is worth noting that even a slight

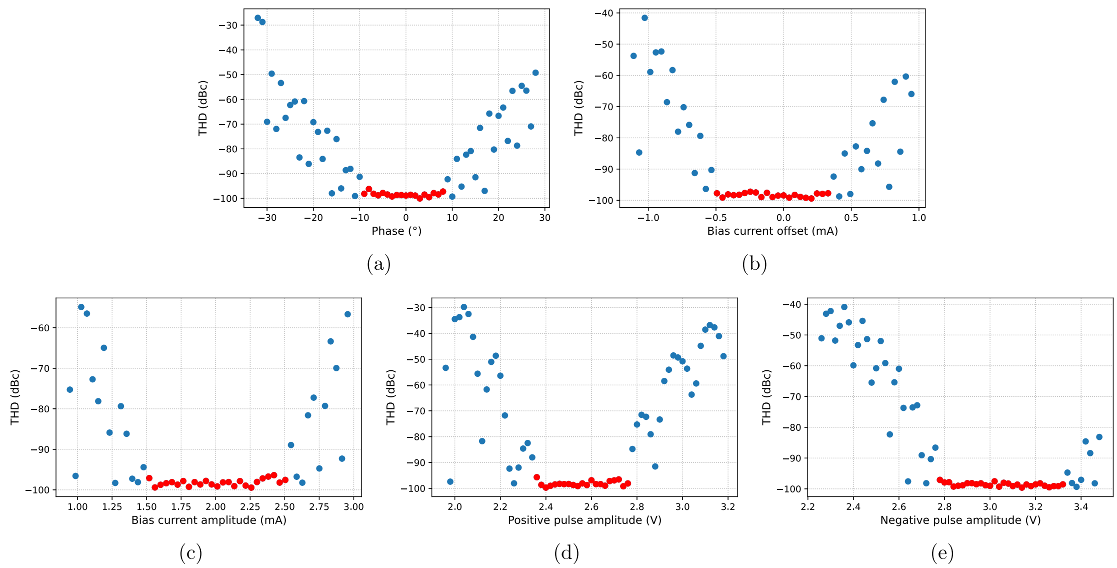

Fig. 8. QLRs of a 30 mV-rms sine wave at 1 kHz. The total harmonic distortion (THD) is plotted as a function of: (a), (b) and (c) phase, offset and amplitude of the compensation current; (d) and (f) positive and negative pulse amplitudes. Red dots represent consecutive parameters values within the QLR, where THD is both minimized (<95 dBc) and quantized.

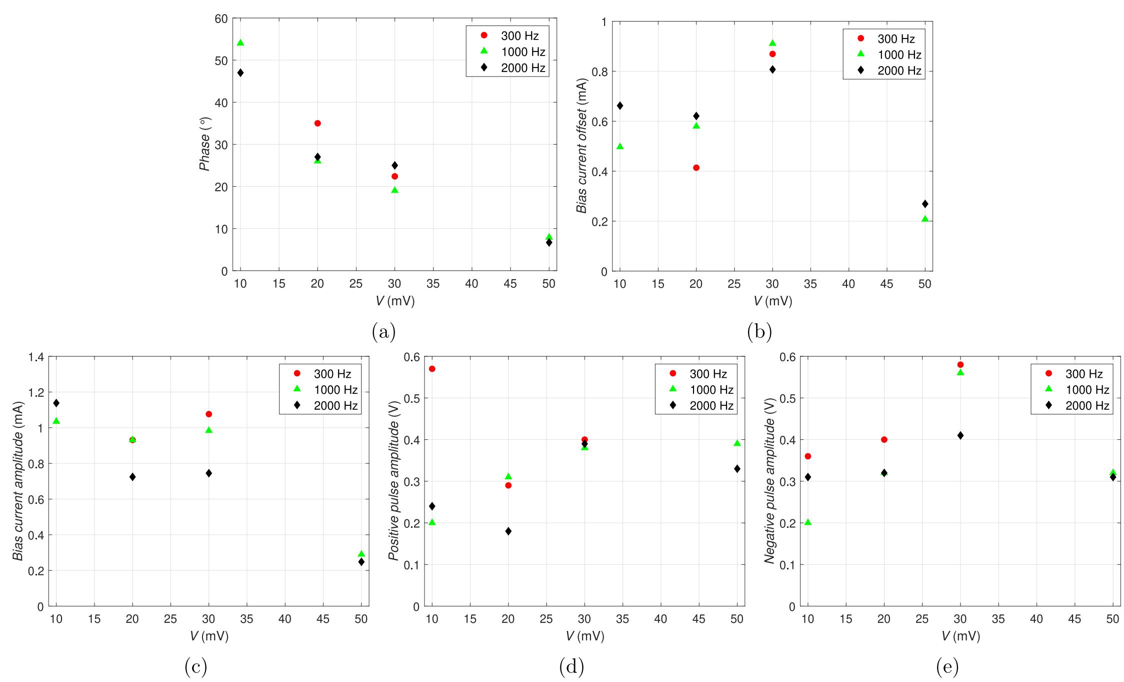

Fig. 9. Width of QLRs of JAWS sine waves under variation of: (a), (b) and (c) phase, offset and amplitude of the compensation current; (d) and (f) positive and negative pulse amplitudes. Note: for the case of 10 mV rms at 300 Hz bias current was not needed.

frequency change of 0.1% results in a significant alteration in the relative difference, particularly at lower voltage levels (10 mV rms and 20 mV rms). The results of JAWS calibrations were also compared with those from a calibration certificate issued by INRiM for the same instrument, traceable to INRiM primary standards through traditional comparisons based on thermal converters. Both sets of results are in good agreement, with the expanded uncertainty calculated for the JAWS system being approximately one order of magnitude lower. This is consistent with a similar outcome reported in a pioneering work [36], where the authors also obtained uncertainty one order of magnitude lower than that from conventional ac-dc calibration for frequencies up to 10 kHz and amplitudes up to 100 mV rms.

The uncertainty budget for the ac voltmeter calibration at 10 mV and 2 kHz is given in Table 1. Type A uncertainty contribution arises from various random effects, including short-term stability of the instruments, as well as thermal and other effects commonly observed in ac-dc transfer. This uncertainty source is voltage dependent, though significantly lower than 0.7 μV/V for all the measured frequencies and voltages. This is in contrast to the results presented in [18] where the uncertainty type A was more than one order of magnitude higher, in spite of using liquid helium to cool the JAWS device. This may be due to Fluke 5790A operates in the measurement mode using internal very stable dc source as a reference for the ac-dc transfer in contrast to Fluke 792A from [18] where the dc and nanovoltmeter must be connected externally. Similar levels of type A uncertainty were achieved in [37],

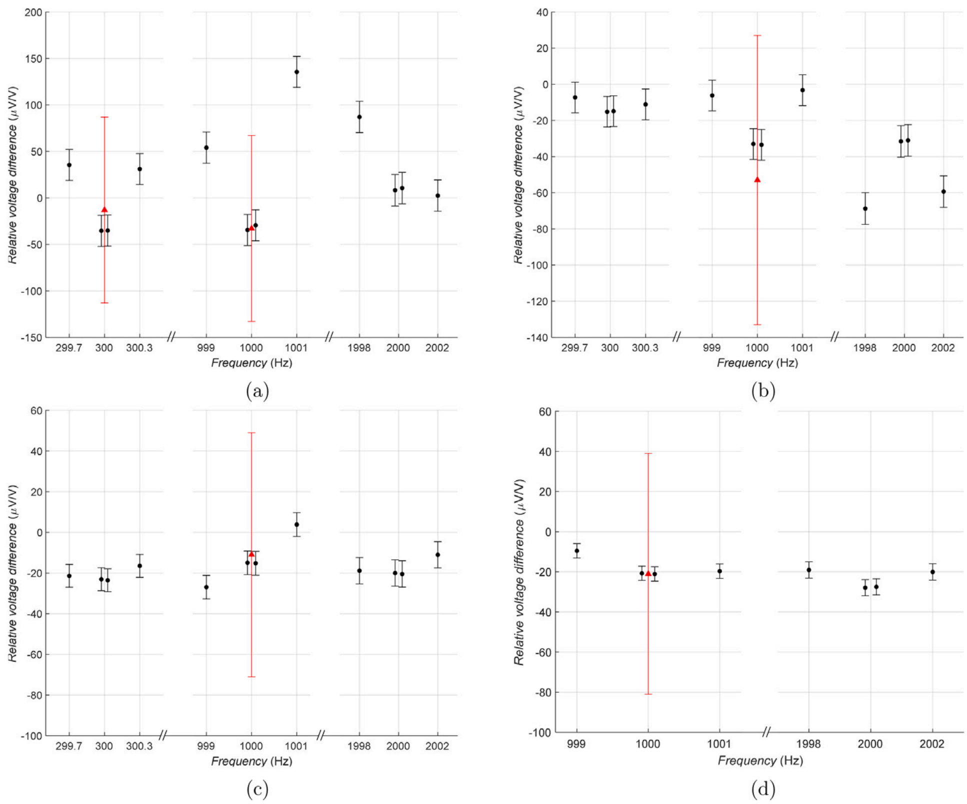

Fig. 10. Calibration results of the true-rms voltmeter for: (a) 10 mV rms (b) 20 mV rms (c) 30 mV rms (d) 50 mV rms with the JAWS (black dots) and thermal voltage converter (red triangles). The results for 300, 1000 and 2000 Hz were slightly shifted for better visibility. Error bars represent the expanded uncertainty (k = 2).

Table 1
Uncertainty budget for the JAWS calibration of the Fluke 5790 ac voltmeter at 10 mV and 2 kHz.

Uncertainty source	Uncertainty ($\mu V\,V^{-1}$)
Type A	
Noise	<0.7
Type B	
Thermoelectric dc voltage	6.0
Electromagnetic interference (EMI)	5.8
On-chip inductance	0.47
Transmission line	<0.01
Combined standard uncertainty (k = 1)	**8.4**

where it amounted to approximately 1.1 μV/V for a synthesized 1 mV rms signal, also utilizing a liquid helium system.

Major type B uncertainty contributions are described as follows. Other type B sources not specified in Table 1, such as $\Sigma\Delta$ modulation, phase noise, and junctions delays, were collectively estimated to be below the level of 0.01 μV/V for all the calibration points under consideration.

5.3.1. Thermoelectric dc voltage

The wideband ac voltmeter Fluke 5790A contains the true-rms thermal converter for conversion of the input voltage to the equivalent thermal power dissipation. This type of converter works not only with ac voltages (sinusoidal) but also with dc and distorted ac signals. In our case, the ac sinusoidal signal generated by the JAWS is biased by the thermoelectric effect while dc is provided internally by Fluke's reference source without this thermoelectric bias. Consequently, thermoelectric effect is not canceled in this ac/dc transfer. The thermoelectric voltage is approximately 470 nV, measured with a Keithley 2182A nanovoltmeter. This value was then subtracted from the output voltage calibration results and the estimated type B uncertainty.

5.3.2. Electromagnetic interference (EMI)

EMI is one of the most important factors in measurement systems consisting of several electronic devices. There are several types of mechanisms contributing to EMI, such as capacitive or inductive couplings, grounding loops, and others. As described, the system was optimized to reduce EMI by utilizing separation transformers, a single grounding point, chokes, and DC blocks to decouple the instruments. Devices not directly involved in measurements, such as computers, ac/dc power supplies, roughing pumps, turbomolecular pumps, cryogenic compressors, etc., were connected to the grid separately from the isolation transformer.

Typically, the simplest method to measure EMI involves turning off all equipment and measuring the residual voltage. However, in the current system, the residual EMI was intended to be measured by the Fluke 5790A, which has a lower limit of 600 μV, while the actual EMI is well below this threshold. Therefore, we explored an alternative method:

1. We measured the dc thermoelectric effect using a Keithley 2182A nanovoltmeter;
2. Next, we synthesized a sinusoidal signal with an rms amplitude of 1 mV at 1 kHz using the JAWS array, for which no compensation current was needed. In this scenario, the voltage measured by the voltmeter comprised a synthesized voltage with a previously determined thermoelectric dc bias and an unknown residual EMI. Together, these components exceeded the lower limit of detection of the voltmeter;
3. Through precise measurement of the 1 mV quantum signal and iterative adjustments to the system, including grounding loop minimization, filter addition, choke integration, and the use of a separation transformer, we identified the configuration that yielded the minimum average voltage as indicated by the Fluke 5790;

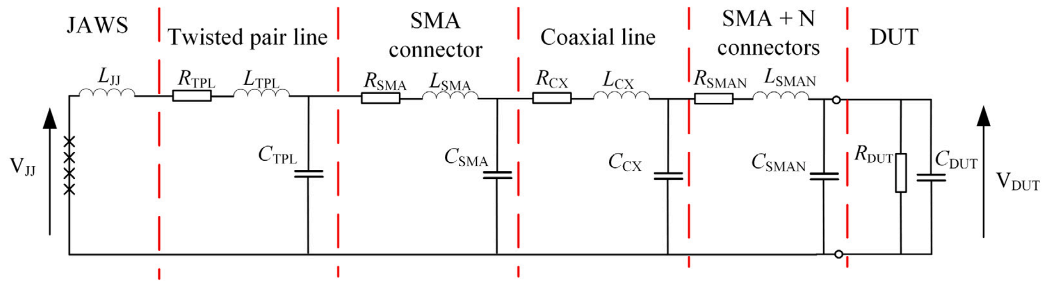

Fig. 11. The equivalent electrical model of the JAWS output connected to the DUT. *R*, *L*, and *C* denote parasitic resistance, inductance, and capacitance, respectively.

4. Upon reaching a stage where further reduction in the measured voltage was unattainable, we computed the residual EMI error by factoring in the synthesized voltage amplitude and dc thermoelectric bias. Any remaining undetectable EMI was presumed to match the resolution of the Fluke device (100 nV rms), subsequently utilized in type B uncertainty calculations.

5.3.3. On-chip inductance

The inductance of the array measured by its manufacturer (Physikalisch-Technische Bundesanstalt, PTB) is approximately 126 nH. The low frequency bias current passing through this array induces the inductive part of the voltage, which is non-quantized. Similar to the cable loading effect, the simple two-port network model of the JAWS allowed for estimating the correction of the output voltage and calculating the type B uncertainty. As displayed in Table 1, the type B uncertainty caused by this effect is approximately 1.4 μV/V at 2 kHz and 10 mV rms.

5.3.4. Transmission line

Finally, the cable-loading effect and the input impedance of the connected DUT play crucial roles in determining the systematic error and type B uncertainty of the calibration system. To reduce their influence on the deterioration of calibration accuracy, any instrument connected to a pulsed standards must be set for high impedance operation. Interconnecting cables are then treated as lumped resistive-capacitive loads by the Josephson device. The connection between the pulsed array and voltmeter must be viewed as a transmission line with resistors and capacitors connected in parallel, significantly altering the synthesized quantum-accurate signal. Despite our cryocooled system significantly reduces the required length of the twisted pair cable inside the dewar, the cable used for winding the choke caused the non-negligible residual loading. The equivalent circuit of the cables from the JAWS to the DUT was prepared in a similar manner to that proposed in [38] and given in the Fig. 11

The input impedance of the DUT is given in its datasheet as resistance 10 MΩ and capacitance 100 pF connected in parallel. This information allowed for calculating the correction (systematic effect) dependent on the frequency, which was then subtracted from the output voltage.

6. Conclusions

A cryocooled pulse-driven Josephson standard setup for the analysis of a commercial thermal converter properties by means of quantized pure sine waves was presented. In particular, the preparation of the measurement apparatus and the optimization of operating parameters for the generation of verified quantum signals were discussed. Despite the visible fluctuations of the cryocooler base temperature, quantum-locking ranges are wide enough to reliably use this system for the direct calibration of the true rms voltmeter.

The results of the calibration by using the designed JAWS system are in a good agreement with these obtained from traditional comparison with Fluke 792A, but the calculated uncertainty is about one order of magnitude lower. Compared with the traditional methods, the direct ac calibration against a JAWS has the advantage of a dramatic reduction of the number of steps in the traceability chain [39], with significant benefits in terms of both accuracy and measurements time. To summarize, the presented system has utmost performance for the direct calibration of the DUT for low voltage range (<50 mV_{rms}) which is the most challenging for the thermal ac/dc transfer. Methods to enhance pulse power capabilities and mitigate inductance effects through zero-current bias will be investigated and implemented, aiming at the extension of both voltage and frequency ranges with reduced uncertainty.

CRediT authorship contribution statement

Krzysztof Kubiczek: Writing – review & editing, Writing – original draft, Visualization, Validation, Methodology, Investigation, Funding acquisition, Formal analysis, Data curation. **Paolo Durandetto:** Writing – review & editing, Writing – original draft, Visualization, Software, Methodology, Investigation, Formal analysis, Data curation, Conceptualization. **Pier Paolo Capra:** Writing – review & editing, Validation, Investigation, Formal analysis. **Claudio Francese:** Writing – review & editing, Validation, Investigation, Formal analysis. **Marco Lanzillotti:** Writing – review & editing, Validation, Investigation, Data curation. **Luca Roncaglione:** Writing – review & editing, Investigation, Formal analysis, Conceptualization. **Marian Kampik:** Writing – review & editing, Supervision, Investigation, Funding acquisition, Formal analysis. **Andrea Sosso:** Writing – review & editing, Writing – original draft, Validation, Supervision, Project administration, Methodology, Investigation, Funding acquisition, Formal analysis, Data curation, Conceptualization.

Declaration of competing interest

The authors declare the following financial interests/personal relationships which may be considered as potential competing interests: Krzysztof Kubiczek reports financial support was provided by National Science Centre Poland. The other authors declare that they have no known competing financial interests or personal relationships that could have appeared to influence the work reported in this paper.

Data availability

No data was used for the research described in the article.

Acknowledgments

This research was partially funded by the Polish National Science Center (NCN) [grant no. 2022/06/X/ST7/00014] and by Rector of Silesian University of Technology, Poland [grant no. 05/020/RGJ24/0084 and 05/020/RGJ23/0078]. The authors are indebted with Dr. O. Kieler of Physikalisch-Technische Bundesanstalt for providing the chips used in this work.

References

[1] M. Stock, R. Davis, E. de Mirandés, M.J. Milton, The revision of the SI – the result of three decades of progress in metrology, Metrologia 56 (2) (2019) 022001.

[2] R. Behr, A.S. Katkov, Final report on the key comparison EUROMET. BIPM. EM-K10. A: Comparison of Josephson array voltage standards by using a portable Josephson transfer standard, Metrologia 42 (1A) (2005) 01005.

[3] V. Lacquaniti, A. Sosso, Josephson junctions for present and next generation voltage metrology, in: Modern Metrology Concerns, InTech, 2012, p. 121.

[4] P. Dresselhaus, Y. Chong, J. Plantenberg, S. Benz, Stacked SNS Josephson junction arrays for quantum voltage standards, IEEE Trans. Instrum. Meas. 13 (2) (2003) 930–933, http://dx.doi.org/10.1109/TASC.2003.814151.

[5] J. Kohlmann, F. Müller, O. Kieler, R. Behr, J. Palafox, M. Kahmann, J. Niemeyer, Josephson series arrays for programmable 10-V SINIS Josephson voltage standards and for Josephson arbitrary waveform synthesizers based on SNS junctions, IEEE Trans. Instrum. Meas. 56 (2) (2007) 472–475.

[6] V. Lacquaniti, C. Cagliero, S. Maggi, R. Steni, Overdamped Nb/Al-AlO$_x$/Nb Josephson junctions, Appl. Phys. Lett. 86 (4) (2005) 04–2501, http://dx.doi.org/10.1063/1.1856135.

[7] V. Lacquaniti, N. De Leo, M. Fretto, S. Maggi, A. Sosso, Nb/Al-AlO$_x$/Nb overdamped Josephson junctions above 4.2 K for voltage metrology, Appl. Phys. Lett. 91 (25) (2007) 252505.

[8] J. Lee, R. Behr, L. Palafox, A. Katkov, M. Schubert, M. Starkloff, A.C. Böck, An ac quantum voltmeter based on a 10 V programmable Josephson array, Metrologia 50 (6) (2013) 612.

[9] M.-S. Kim, H. Cho, R. Chayramy, S. Solve, Measurement configurations for differential sampling of ac waveforms based on a programmable Josephson voltage standard: effects of sampler bandwidth on the measurements, Metrologia 57 (6) (2020) 065020.

[10] Y. Amagai, M. Maruyama, N. Sakamoto, T. Shimazaki, H. Yamamori, H. Fujiki, N.-H. Kaneko, Sampling measurement of a 20-v rms sine wave using an inductive voltage divider and an ac-programmable Josephson voltage standard, in: 2018 Conference on Precision Electromagnetic Measurements, CPEM 2018, IEEE, 2018, pp. 1–2.

[11] A. Rüfenacht, C.J. Burroughs, P.D. Dresselhaus, S.P. Benz, Differential sampling measurement of a 7 V RMS sine wave with a programmable Josephson voltage standard, IEEE Trans. Instrum. Meas. 62 (6) (2013) 1587–1593.

[12] R. Behr, L. Palafox, An ac quantum voltmeter for frequencies up to 100 khz using sub-sampling, Metrologia 58 (2) (2021) 025010.

[13] R. Behr, A. Katkov, J. Lee, S. Bauer, O. Kieler, L. Palafox, Frequency range extension of the AC quantum voltmeter, in: 2018 Conference on Precision Electromagnetic Measurements, CPEM 2018, 2018, pp. 1–2, http://dx.doi.org/10.1109/CPEM.2018.8501156.

[14] K.I. WG, R. Landim, Investigations on extending the frequency range of PJVS based AC voltage calibrations by coherent subsampling, in: 2016 Conf. on Precision Electromagnetic Measurements, CPEM, 2016.

[15] J. Kim, A. Sosso, A.F. Clark, Dynamics of overdamped Josephson junctions driven by a square-wave pulse, J. Appl. Phys. 83 (6) (1998) 3225–3232.

[16] S. Benz, C. Hamilton, A pulse-driven programmable Josephson voltage standard, Appl. Phys. Lett. 68 (22) (1996) 3171–3173.

[17] S. Pavan, R. Schreier, G.C. Temes, Understanding Delta-Sigma Data Converters, John Wiley & Sons, 2017.

[18] J.M. Underwood, Uncertainty analysis for ac–dc difference measurements with the AC Josephson voltage standard, Metrologia 56 (1) (2018) 015012.

[19] K. Kubiczek, M. Kampik, M. Grzenik, Analysis of DC reversal error of the calorimetric thermal voltage converter, Measurement 168 (2021) 108439, http://dx.doi.org/10.1016/j.measurement.2020.108439.

[20] K. Kubiczek, M. Kampik, M. Grzenik, A novel temperature sensor for a calorimetric thermal converter, Measurement 201 (2022) 111686, http://dx.doi.org/10.1016/j.measurement.2022.111686.

[21] A. Sosso, P. Durandetto, B. Trinchera, O. Kieler, R. Behr, J. Kohlmann, Characterization of a Josephson array for pulse-driven voltage standard in a cryocooler, Measurement 95 (2017) 77–81, http://dx.doi.org/10.1016/j.measurement.2016.09.039.

[22] P. Durandetto, E. Monticone, D. Serazio, A. Sosso, Thermal performances of an improved package for cryocooled Josephson standards, IEEE Trans. Compon. Packag. Manuf. Technol. 9 (7) (2019) 1264–1270.

[23] J. Kohlmann, O. Kieler, R. Iuzzolino, J. Lee, R. Behr, B. Egeling, F. Muller, Development and investigation of SNS Josephson arrays for the Josephson arbitrary waveform synthesizer, IEEE Trans. Instrum. Meas. 58 (4) (2009) 797–802, http://dx.doi.org/10.1109/TIM.2008.2007033.

[24] O. Kieler, T. Scheller, J. Kohlmann, Cryocooler operation of a pulse-driven AC Josephson voltage standard at PTB, World J. Condens. Matter Phys. 3 (2013) 189–193.

[25] P. Durandetto, A. Sosso, Using a Josephson junction as an effective on-chip temperature sensor, Supercond. Sci. Technol. 34 (4) (2021) 045008.

[26] S. Bauer, R. Behr, J. Herick, O. Kieler, M. Kraus, H. Tian, Y. Pimsut, L. Palafox, Josephson voltage standards as toolkit for precision metrological applications at PTB, Meas. Sci. Technol. 34 (3) (2022) 032001.

[27] S. Benz, C. Burroughs, P. Dresselhaus, AC coupling technique for Josephson waveform synthesis, IEEE Trans. Appl. Supercond. 11 (1) (2001) 612–616.

[28] E. Houtzager, S.P. Benz, H.E. van den Brom, Operating margins for a pulse-driven Josephson arbitrary waveform synthesizer using a ternary bit-stream generator, IEEE Trans. Instrum. Meas. 58 (4) (2009) 775–780.

[29] A. Rüfenacht, N.E. Flowers-Jacobs, S.P. Benz, Impact of the latest generation of Josephson voltage standards in ac and dc electric metrology, Metrologia 55 (5) (2018) S152.

[30] A. Sosso, P. Durandetto, Experimental analysis of the thermal behavior of a GM cryocooler based on linear system theory, Int. J. Refrig. 92 (2018) 125–132, http://dx.doi.org/10.1016/j.ijrefrig.2018.04.016.

[31] R. Webber, J. Delmas, Cool-down acceleration of GM cryocoolers with thermal oscillations passively damped by helium, in: IOP Conference Series: Materials Science and Engineering, Vol. 101, IOP Publishing, 2015, 012137.

[32] N.E. Flowers-Jacobs, A.E. Fox, P.D. Dresselhaus, R.E. Schwall, S.P. Benz, Two-volt Josephson arbitrary waveform synthesizer using Wilkinson dividers, IEEE Trans. Appl. Supercond. 26 (6) (2016) 1–7.

[33] S.P. Benz, S.B. Waltman, A.E. Fox, P.D. Dresselhaus, A. Rüfenacht, J.M. Underwood, L.A. Howe, R.E. Schwall, C.J. Burroughs, One-volt Josephson arbitrary waveform synthesizer, IEEE Trans. Appl. Supercond. 25 (1) (2014) 1–8.

[34] W. Kester, Data Conversion Handbook, Newnes, 2005.

[35] H.E. Van den Brom, E. Houtzager, Voltage lead corrections for a pulse-driven ac Josephson voltage standard, Meas. Sci. Technol. 23 (12) (2012) 124007.

[36] T.E. Lipe, J.R. Kinard, Y.-H. Tang, S.P. Benz, C.J. Burroughs, P.D. Dresselhaus, Thermal voltage converter calibrations using a quantum ac standard, Metrologia 45 (3) (2008) 275, URL http://stacks.iop.org/0026-1394/45/i=3/a=003.

[37] D. Georgakopoulos, I.F. Budovsky, S.P. Benz, Evaluation of a Josephson arbitrary waveform synthesizer at low voltages for the calibration of lock-in amplifiers, IEEE Trans. Instrum. Meas. 70 (2021) 1–7.

[38] P.S. Filipski, J.R. Kinard, T.E. Lipe, Y.-H. Tang, S.P. Benz, Correction of systematic errors due to the voltage leads in an AC Josephson voltage standard, IEEE Trans. Instrum. Meas. 58 (4) (2008) 853–858.

[39] U. Pogliano, G.C. Bosco, V. D'Elia, Extension of the IEN traceability for ac voltages below 200 mV, IEEE Trans. Instrum. Meas. 52 (2) (2003) 375–379.